Journal of Electroanalytical Chemistry 810 (2018) 222–231

Contents lists available at ScienceDirect

Journal of Electroanalytical Chemistry

journal homepage: www.elsevier.com/locate/jelechem

Oxygen reduction electrocatalysis on transition metal-nitrogen modified tungsten carbide nanomaterials

Ulisses Alves do Rêgo[a,b], Thiago Lopes[a,*], José Luiz Bott-Neto[a], Auro Atsushi Tanaka[b], Edson Antonio Ticianelli[a]

[a] Instituto de Química de Sao Carlos, Universidade de Sao Paulo, 13560-960 Sao Carlos, SP, Brazil
[b] Universidade Federal do Maranhao, 65080-040 Sao Luis, MA, Brazil

ARTICLE INFO

Keywords:
Oxygen reduction reaction
Carbide
Carbide-metal-nitrogen/C catalysts
Energy conversion and storage

ABSTRACT

Considering the technological importance of the oxygen reduction reaction (ORR) and the cost constraints of highly catalytically active precious metals, recent research efforts have been focused on designing and synthesizing earth abundant non-precious metal catalysts for this reaction. Among recent advances in this area, transition metal-nitrogen modified tungsten carbides can be pointed as prominent candidates as ORR electrocatalysts. Nevertheless, mechanistically understandings of which active sites are responsible for the ORR electrocatalysis on these materials are required for the rational design of suitable materials. In the present work, various tungsten carbides and iron-nitrogen modified tungsten carbides catalysts are synthesized and in-depth characterized through various physical and electrochemical techniques towards gaining insights on the ORR process on these materials in both acidic and alkaline media. High performance materials are developed, with the most active presenting only a ca. 0.060 V increase in the ORR overpotential, compared to a standard platinum catalyst in an alkaline medium. The in-depth analyses allowed for suggestions on reaction pathways for the oxygen reduction on the hybrid Fe/N/WC/C nanomaterials in terms of active sites. These finds might direct further developments in the research on transition metal-nitrogen modified tungsten carbide materials.

1. Introduction

Tungsten carbide may be referred to as an interstitial alloy, [1] possessing electronic and catalytic properties known from the group VIII B precious metals, such as palladium and platinum [2, 3]. Tungsten carbide tends to present considerable catalytic activity attributed to a distinct electronic structure promoted by the presence of carbon in the metal lattice and to its platinum-like characteristic in terms of chemisorption of hydrogen and oxygen [4–6]. Considering its reduced price versus precious metals [7] and its interesting chemisorption properties, tungsten carbide has been investigated as hydrogen oxidation and oxygen reduction catalyst in acidic pHs, with limited studies in alkaline medium [8].

Given the cost constraints on the use of precious metals to catalyze the technological oxygen reduction reaction (ORR), recent research efforts have aimed at a rational design to synthesize non-precious metal catalysts (NPMCs), based on earth abundant elements. As range of such NMPCs has been developed, including heteroatom-doped carbonaceous materials (e.g. N/C), non-precious metal oxides, nitrides, carbides and transition metal-N/C catalysts, such as FeN_x/C [9–11]. Among these, transition metal-N/C and tungsten carbide catalysts show promising potential, although at the present stage of development, their intrinsic electroanalytic activities are low compared to platinum [12–14]. Due to its low catalytic activity towards the ORR in acid media, compared to precious metals, tungsten carbide has mainly been investigated as a support to promote the catalytic activity of precious metals [14]. However, a few recent studies have indicated the high ORR catalytic activity of transition metal/nitrogen-modified tungsten carbide catalysts, [15–19] although only in alkaline medium.

Despite the high ORR activity of these catalysts at high pH values, there have been no mechanistic investigations with the aim of understanding the active sites responsible for the electrocatalysis of oxygen reduction, in order to produce suitable materials. Investigations of such catalysts for the oxygen reduction reaction have mostly been limited to using alkaline media, in which only nitrogen doped carbon materials have been shown to present a high catalytic activity, [11] which makes it difficult to discern the advantage of transition metal-nitrogen modified tungsten carbide catalysts. In the present work, a series of tungsten carbide and iron/nitrogen-modified tungsten carbide catalysts were synthesized and were submitted to an in-depth characterization using

* Corresponding author at: Instituto de Pesquisas Energéticas e Nucleares, IPEN/CNEN-SP, 05508-000 Sao Paulo, SP, Brazil.
E-mail addresses: ulisses.alves@ufma.br (U.A. do Rêgo), thiago.lopes@ipen.br (T. Lopes), tanaka.auro@ufma.br (A.A. Tanaka), edsont@iqsc.usp.br (E.A. Ticianelli).

https://doi.org/10.1016/j.jelechem.2018.01.013
Received 17 October 2017; Received in revised form 11 December 2017; Accepted 6 January 2018
Available online 09 January 2018
1572-6657/

various physical and electrochemical techniques, in order to gain insights into the oxygen reduction reaction process on these hybrid materials in both acidic and alkaline media, where suitably ORR active materials are achieved with about only 0.063 V of difference in the ORR half wave potential to a standard platinum catalyst in alkaline medium. Furthermore, the in-depth analyses carried out allowed for propositions on the oxygen reduction reaction pathways on the hybrid materials in terms of active sites, which should assist in the rational development of tailored highly-active ORR transition metal/nitrogen-modified tungsten carbide catalysts.

2. Experimental

2.1. Synthesis of the catalysts

Analytica grade chemicals were utilized in this work without further purification. Tungsten carbide was synthesized following a procedure described in the literature procedure [20]. Briefly, proportional masses of WO_3 (99,5% Sigma-Aldrich) and carbon black (Vulcan XC-72, Cabot-Corp) at WC:C percentages of 20, 30 and 40% were added to 300 mL and to 100 mL of ethanol (98%, PanReac AppliChem), respectively, and the mixtures were placed in an ultrasonic bath for 1 h. Subsequently, the two mixtures were combined and then left in an ultrasonic bath for 2 h, after which, this mixture was placed on a hot plate and the temperature was adjusted to 90 °C in order to promote the evaporation of the solvent. The dried powder was transferred to an alumina boat, which was placed in a quartz tube and heated in a tubular oven (Model FT 1300/H, INTI). The temperature of the oven was raised at 5 °C min^{-1} to reach 850 °C, at which it was maintained for 4 h with a controlled gas atmosphere of CH_4/H_2 (1:1 v/v) in the quartz tube. After this heating treatment, the temperature was brought to about 25 °C and the as synthesized WC/C was passivated for 12 h in an atmosphere composed of 1% oxygen in an air/argon mixture (1:20 v/v).

As a source of iron and nitrogen sources for the synthesis of FeN_x-WC/C, a metal macrocyclic complex was prepared as follows: 20 mL of a 0.003 mol L^{-1} solution of 2,4,6-Tris(2-pyridyl)-1,3,5-triazine (TPTZ ≥ 99% from Sigma-Aldrich) in 60/40 v/v ethanol and hydrochloric acid (0.2 mol L^{-1}) was added to 300 mL of ammonium iron(II) sulfate hexahydrate (99% Sigma-Aldrich) 0.050 mol L^{-1} in DI water (18.2 MΩ cm), where the iron to TPTZ ratio was 1:2.1. Following addition of the iron salt, the solution became violet, indicating the formation of the $[Fe(TPTZ)_2]^{2+}$ complex, as confirmed by UV–Vis spectroscopy (Section 2.2). This solution was left under stirring for 2 h to complete the complexation and was then stored before further use. For the synthesis of the FeN_x-WC/C catalysts, 1 g of the (WC/C) support was added to 300 mL of ethanol (PanReac AppliChem), together with the referent aliquot of the $[Fe(TPTZ)_2]^{2+}$ complex corresponding to an iron to WC/C ratio of 5 wt%. This solution was left under stirring for 24 h, after which, the temperature of the solution was increased to 90 °C to evaporate the solvent. The dried solid was transferred to an alumina boat and placed in a quartz tube in a tubular oven under an inert atmosphere of N_2 (130 mL min^{-1}). Pyrolysis was carried out for 2 h at 700 or 800 °C, using a heating ramp of 5 °C min^{-1}. The material was allowed to cool to ambient temperature and the catalyst was ready to use. The synthesized catalysts were denoted WC(20)-FeN_x/C(700), WC(20)-FeN_x/C(800), WC(30)-FeN_x/C(700), WC(30)-FeN_x/C(800), WC(40)-FeN_x/C(700) and WC(40)-FeN_x/C(800), where values within the first parentheses is the weight percentage of WC:C in the support and the number within the second parentheses is pyrolisis temperature.

2.2. Physical characterization of the catalysts

The formation of the $[Fe(TPTZ)_2]^{2+}$ complex was confirmed by UV–Vis spectroscopy (UV 3600 from Shimadzu) in a quartz cuvette with an optical pathway of 1 cm. A typical spectrum obtained is shown in Fig. S1, which presents a peak at 593 nm with a shoulder at 532 nm, in suitable agreement with the literature [21]. X-ray diffraction measurements of catalysts were carried out in a Rigaku Rotaflex, model Ru200B, with the tube at 40 kV and 40 mA with a target of Cu (λ.kα = 1,5406 Å), between 10° and 90° at a scan rate of 1° per minute. Elemental analysis was carried out in a scanning electron microscope from Zeiss, model LEO 440/20 keV electron beam and equipped with a EDX microanalyser (Link Analytical, Isis System Series 200) with a SiLi Pentafet detector. Transmission electron microscopy analyses were carried out in a 200 kV JEOL-JEM2100 equipment. X-ray photoelectron spectroscopy results of selected catalysts were obtained in a K-Alpha XPS from Thermo Scientific with a 180° double focusing hemispherical analyzer-128-channel detector and an Al Ka Micro-focused X-ray monochromator. To obtain the XPS spectra, the equipment was programmed with the following configurations: passage of 20 eV, energy step of 0.1 eV, and acquisition time of 200 ms. The survey and high-resolution spectra of elements were collected with pass energy and energy step of 1.0 eV and 0.1 eV, respectively. The XPS results were fitted using Gaussian-Lorentzian function and Shirley background and all binding energy of catalyst were adjusted using carbon peak (C 1s) at 284.8 eV. Assignments of the bindings energies resulting from the fittings of high resolution XPS scans were made in accordance to the literature: [20, 21] for WC and WO_3 [22, 23, 24–26] for WO_2; [27] for WS_2; [28] for pyridinic, pyrrolic, graphitic and oxidized nitrogen species; and [29] for the Fe^{3+} species.

2.3. Electrochemical measurements

A rotating ring-disk electrode, with a glassy carbon disk (0.196 cm^2) and a gold ring (model AFE6R1AU), a MSR rotator, both from Pine Instruments, and a bipotentiostat, from Autolab (PGSTAT 30) were utilized in the electrochemical characterization of the activity of synthesized catalysts towards the oxygen reduction reaction. A three-electrode glass cell with a reversible hydrogen (RHE) reference electrode with a platinum wire junction to the test solution, and a 2 cm^2 gold foil counter electrode was used. Electrolyte solutions were prepared by dilution of concentrated reactants to the necessary degree, or 0.5 mol L^{-1} H_2SO_4 (96%, PanReac AppliChem) and 0.1 mol L^{-1} NaOH (99% Merk) with DI water (18.2 MΩ cm). To form the working electrode, the catalysts were deposited on the glassy carbon disk as per a procedure described in the literature [30, 31]. The temperature of the electrolyte solutions was maintained at 25 ± 0.1 °C by recirculating water through the jacket of the electrochemistry glass cell with a thermostat recirculating bath (Cole-Parmer). Electrolyte solutions were saturated either with pure oxygen (99.999%, White Martins) or with pure argon (99.999% White Martins) through a glass tube having a porous frit tip. To assess the activity of synthesized catalysts towards the oxygen reduction reaction, steady-stated polarization measurements were carried out potentiostatically at a scan rate of the working electrode of 1 mV s^{-1} or of 5 mV s^{-1} under a step height of 30 mV and a waiting time of 30 s per step. For assessing (directly) the formation of hydrogen peroxide in the course of the ORR on the disk, the gold ring of the RRDE was maintained at 1.5 V, which is a potential sufficient to oxidize this molecule under mass transport control. The percentages of hydrogen peroxide formed in the oxygen reduction reaction on the various catalysts were calculated based on both, disk and ring currents, and the collection efficiency of the RRDE electrode, according to [32, 33]:

$$n = 4I_D/(I_D + (I_R/N)) \quad (1)$$

$$\%H_2O_2 = 100(4 - n)/2 \quad (2)$$

where I_D is the Faradaic current at the disk and I_R the current at the ring of the RRDE electrode, and N is the collection efficiency of the electrode.

3. Results and discussion

3.1. Physical characterization

X-ray diffraction patterns of the synthesized catalysts and the tungsten carbide standard (PDF# No. 89-2727) are shown in Fig. 1a and b, where the results strongly suggest the formation of the WC structure in the synthesized materials [34, 35]. It is noteworthy that the peak at about 25° corresponds to the (002) diffraction line of turbostratic-carbon structures (i.e. carbon black), [36–38], with the intensity decreasing in the order WC(20)/C < WC(30)/C < WC(40)/C, in agreement with the increase in the proportion of tungsten carbide to carbon ratio (Table S1). These tungsten carbides have been used as starting materials for the syntheses of hybrid electrocatalysts, [28, 39, 40] and for the targeted incorporation of FeN_x/C and N/C structures, which are also known to be suitably active towards the oxygen reduction reaction in a range of pH values [31, 41–46]. The XRD diffraction patterns of the synthesized hybrid catalysts (WC-FeN_x) are presented in Fig. 1b, together with the standard patterns for tungsten carbide (PDF# No. 89-2727) and ferberite ($FeWO_4$, PDF# No. 46.1446) [47]. The latter was included in this graph because its identified presence was identified in some of the electrocatalysts, as evidenced by the coinciding lines in the diffractograms. The XRD patterns shown in Fig. 1b indicated that the WC(30)-FeN_x/C(700) electrocatalyst contained the least amount of $FeWO_4$.

Fig. 1c and d present transmission electron micrographs of the most ORR active electrocatalysts within its category, along with the respective EDX spectrum used for compositional analysis as insert graph. The results in Fig. 1c and d clearly indicated that the carbon and WC particles cannot be distinguished from each other, and that they probably present not too far sizes. This is in agreement with the values of crystallite sizes of WC calculated from XRD data using the Scherrer equation (Table S2), which is close to 10–20 nm, while the average particle sizes illustrated in the micrograph of Fig. 1d were around 20–30 nm (Fig. S2). This last range is similar to the average size of the primary particles of the carbon black utilized here (Vulcan XC-72) [48].

Elemental analyses of the WC(30)/C and WC(30)-FeN_x/C synthesized materials were performed using X-ray photoelectron spectroscopy (XPS) for. The results obtained by EDX and XPS are provided in Tables S1 and 1, respectively. Comparison of the XPS and EDX data was used to obtain insights into the surface and inner particle chemical compositions of these catalysts. This comparison was carried out for the catalysts most active for the oxygen reduction reaction, WC(30)/C and WC(30)-FeN_x/C, where the latter presented the least amount of $FeWO_4$ (Fig. 1b), so iron would be minimally present as ferberite particles [41]. In comparison to the EDX results (Table S1), the XPS data given in Table 1 indicated much smaller amounts of both tungsten and iron on the surface of the nanoparticles, suggesting that much higher proportions of these transition metals were located in the cores of the particles, rather than on the surfaces.

Deconvolution of the XPS peaks for tungsten, iron and nitrogen provided further information about the chemistry of the synthesized catalysts (Fig. 2). Tungsten was predominantly present as WC in the WC(30)/C catalyst, which contained a much reduced amount of WO_x, [22, 23, 49–51] which is advantageous since WC is more stable than the W_2C phase in electrolytes over a wide range of pH values [52, 53]. However, during the incorporation of FeN_x/C and N/C in the structures, a significant amount of tungsten is oxidized to WO_3 from the original

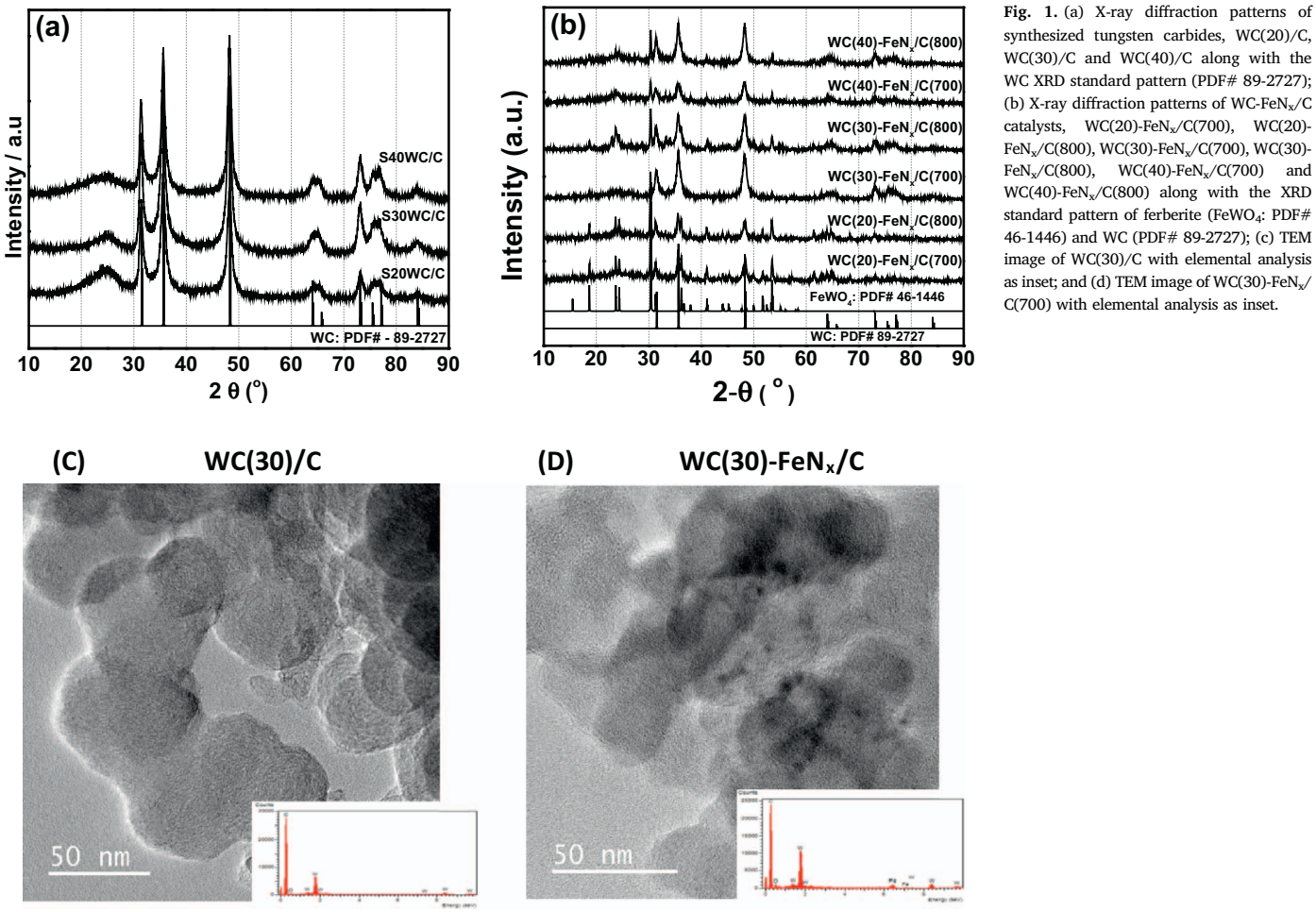

Fig. 1. (a) X-ray diffraction patterns of synthesized tungsten carbides, WC(20)/C, WC(30)/C and WC(40)/C along with the WC XRD standard pattern (PDF# 89-2727); (b) X-ray diffraction patterns of WC-FeN_x/C catalysts, WC(20)-FeN_x/C(700), WC(20)-FeN_x/C(800), WC(30)-FeN_x/C(700), WC(30)-FeN_x/C(800), WC(40)-FeN_x/C(700) and WC(40)-FeN_x/C(800) along with the XRD standard pattern of ferberite ($FeWO_4$: PDF# 46-1446) and WC (PDF# 89-2727); (c) TEM image of WC(30)/C with elemental analysis as inset; and (d) TEM image of WC(30)-FeN_x/C(700) with elemental analysis as inset.

Table 1
C 1s, W 4f, N 1s, and O 1s binding energies (eV) and atomic composition (%) of WC/C, WC(30)-FeNx/C(700), and WC(30)-FeNx/C(800) catalysts determined by XPS analyses.

	Atomic composition from XPS survey scan				
	C 1 s	O 1 s	W 4f	N 1 s	Fe 2p
WC(30)/C	98.8%	0.9%	0.3%	–	–
WC(30)-FeN_x/C(700)	92.1%	4.6%	0.5%	2.6%	0.4%
WC(30)-FeN_x/C(800)	93.1%	3.6%	0.5%	2.1%	0.8%

	Data from high resolution XPS scans					
	WC (W^{4+} $4f_{7/2}$)	WC (W^{4+} $4f_{5/2}$)	WO_2 (W^{4+} $4f_{7/2}$)	WO_2 (W^{4+} $4f_{5/2}$)	WO_3 (W^{6+} $4f_{7/2}$)	WO_3 (W^{6+} $4f_{5/2}$)
WC(30)/C	44% (32.2 eV)	42% (34.3 eV)	3% (35.0 eV)	4% (37.0 eV)	3% (35.9 eV)	4% (38.3 eV)
	WC (W^{4+} $4f_{7/2}$)	WC (W^{4+} $4f_{5/2}$)	WS_2 (W^{4+} $4f_{7/2}$)	WS_2 (W^{4+} $4f_{7/2}$)	WO_3 (W^{6+} $4f_{7/2}$)	WO_3 (W^{6+} $4f_{5/2}$)
WC(30)-FeN_x/C(700)	8% (32.2 eV)	9% (34.3 eV)	3% (33.2 eV)	2% (35.4 eV)	40% (35.8 eV)	38% (37.9 eV)
WC(30)-FeN_x/C(800)	3% (32.2 eV)	5% (34.3 eV)	1% (33.2 eV)	2% (35.4 eV)	43% (35.9 eV)	46% (38.1 eV)
	Pyridinic (N 1s)	Pyrrolic (N 1s)	Graphitic (N 1s)	Oxidized (N 1s)		
WC(30)-FeN_x/C(700)	43% (398.9 eV)	5% (400.3 eV)	41% (400.9 eV)	11% (402.3 eV)		
WC(30)-FeN_x/C(800)	37% (398.9 eV)	4% (400.3 eV)	49% (400.9 eV)	10% (402.3 eV)		
	Fe^{2+} ($2p_{3/2}$)	Fe^{3+} ($2p_{3/2}$)	Fe^{2+} satellite	Fe^{3+} satellite		
WC(30)-FeN_x/C(700)	28% (710.1 eV)	72% (711.9 eV)	(715.3 eV)	(718.1 eV)		
WC(30)-FeN_x/C(800)	26% (710.5 eV)	74% (711.8 eV)	(715.2 eV)	(718.2 eV)		

WC form (Table 1 and Figs. S3 and S4). It should be noted that WO_3 is largely inactive towards the ORR in both acid and alkaline media, and that it also dissolves in the latter [54–56]. It is noteworthy that most metal carbides, including WC, have been mostly investigated towards the hydrogen oxidation reaction and oxygen reduction reaction in acidic fuel cells. Even though the alkaline media present intrinsic advantage in ORR kinetics, limited electrocatalytic studies have been conducted in alkaline solution [8]. Nevertheless, WC has been extensively investigated as an activity promoter of precious metals towards the oxygen reduction reaction, especially in acidic media [57]. However, least attention has been given to the ORR on the tungsten carbide itself in terms of reaction mechanism and its implications to the overall oxygen reduction reaction on, e.g. Pt/WC, which is discussed in Section 3.2.1 of this work. Furthermore, understanding the origins of the ORR activity of tungsten carbide prepared with nitrogen sources, in terms of active sites, is not well stablished or not discussed in the literature [58–60]. However, this would be important to be understood in order to rationally design highly active ORR specific active sites, which is a matter discussed in Section 3.2.2.

Fig. 2e shows a high-resolution N 1s XPS spectrum of the WC(30)-FeN_x/C electrocatalyst tentatively deconvoluted into different bands corresponding to pyridinic, pyrrolic, graphitic and oxidized nitrogen [42, 61–65]. These nitrogen species lead to different chemical and electronic environments of the neighboring carbon atoms, resulting in different electrocatalytic activities, with the presence of pyridinic and graphitic nitrogen being considered essential for the ability of the material to catalyze the oxygen reduction reaction. However, in recent work, Guo et al. found that that in an acidic medium, pyridinic nitrogen was the active site for ORR, rather than graphitic nitrogen, [66] while in an alkaline medium the catalytic activity was in the order pyridinic-N > pyrrolic-N > graphitic-N > oxidized-N [67]. Pyridinic and pyrrolic nitrogen reduce oxygen via four electrons to water, though graphitic and oxidized nitrogen would reduce oxygen to hydrogen peroxide [67, 68]. Deconvolution of the N 1s peaks in Fig. 2e resulted in percentage distributions of 43%, 5%, 41% and 11% for pyridinic, pyrrolic, graphitic and oxidized nitrogen species, respectively in the WC(30)-FeN_x/C catalyst pyrolyzed at 700 °C. This distribution differed slightly from that for the catalyst pyrolyzed at 800 °C (Table 1 and Fig. S4b). As reported previously, [67] this information is important for interpreting the ORR activities of these electrocatalysts, since different percentages of pyridinic and graphitic nitrogen species in the materials pyrolyzed at different temperatures lead to different ORR catalytic activities at different pHs (see Section 3.2.2).

Recent studies of FeN_x/C species active for the ORR found that in acidic media, the FeN_4/C type site was the most active, [41, 43, 69, 70] and that sites of the FeN_x/C family were far more active than those of the metal free N/C family in acid medium [42, 43]. However, in a recent insightful paper by Malko et al. [43] it was shown that both of these ORR active site familes co-existe in pyrolized Fe/N/C nanostructures, with the results of the electrochemical analysis strongly

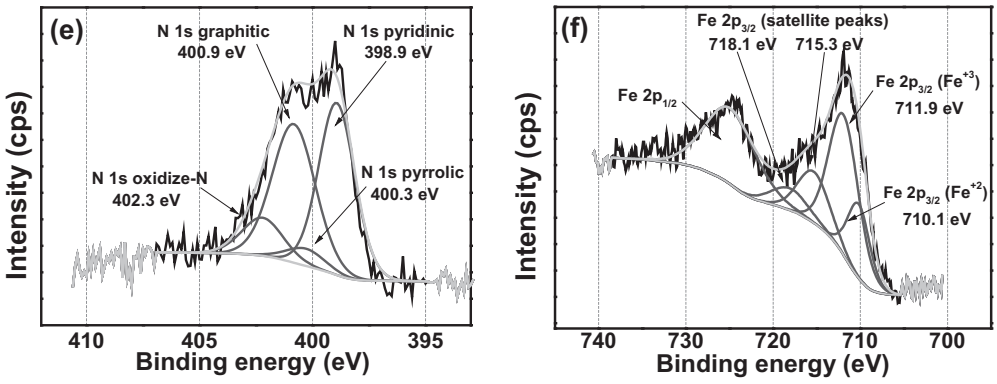

Fig. 2. X-ray photoelectron spectroscopy (XPS) spectra of WC(30)/C (a): wide scan spectrum; and (b) high resolution W4f spectrum with peaks deconvoluted into WC, WO_2 and WO_3. For WC(30)-FeN_x/C: (c) wide scan spectrum; (d) high resolution W 4f spectrum with peaks deconvoluted into WC, WO_3 and WS_2; (e) high resolution N 1s spectrum with the peaks deconvoluted into pyridinic, graphitic/quaternary and oxidized nitrogen species; (f) high resolution Fe 2p spectrum with peaks deconvoluted into Fe^{2+} and Fe^{3+} species.

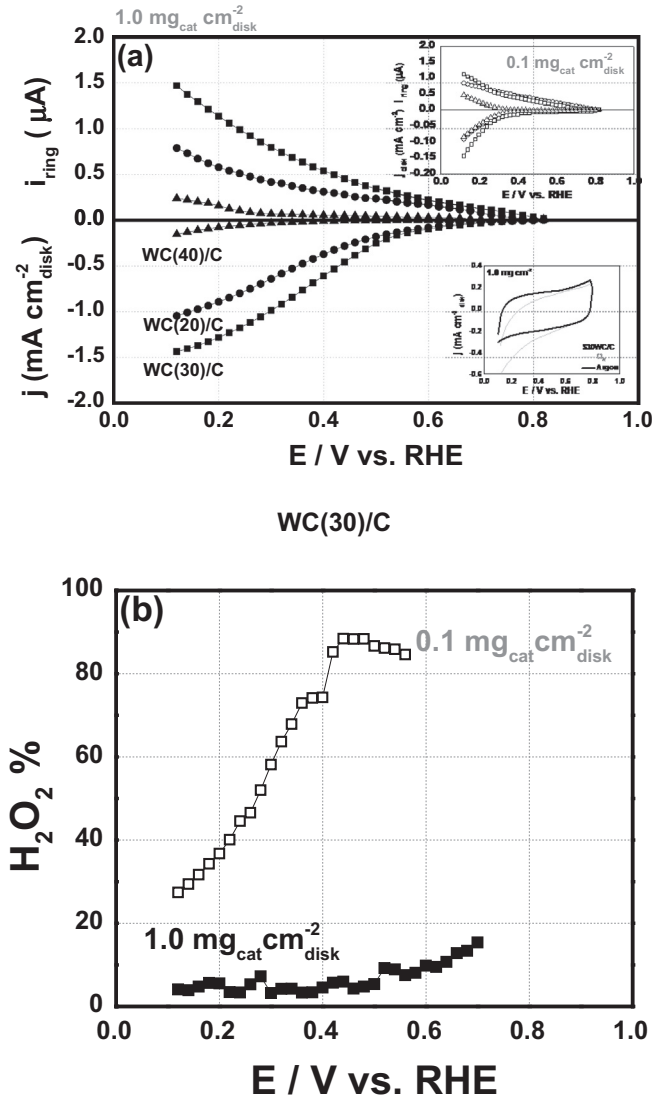

Fig. 3. Electrochemical characterization of WC(20)/C, WE(30)/C and WC(40)/C in 0.5 mol L^{-1} H_2SO_4 at two mass loads in the disk: 0.1 mg_{cat} cm^{-2}_{disk} and 1.0 mg_{cat} cm^{-2}_{disk}: (a) ring/disk currents for 1 mg_{cat} cm^{-2}_{disk} catalyst loading; inset, top: corresponding results for 0.1 mg_{cat} cm^{-2}_{disk}; inset, down: cyclic voltammogram for WC(30)/C (0.1 mg_{cat} cm^{-2}_{disk}), v = 20 mV s^{-1}; (b) percentage of hydrogen peroxide detected on the ring for the WC(30)/C catalyst at both low and high catalyst loadings. RRDE experiments performed at a scan rate (v) of 1 mV s^{-1}; w = 400 rpm, T = 25.0 ± 0.1 °C.

suggesting that the metal-free N/C family of active sites could be solely responsible for the ORR catalytic activity of the pyrolized Fe/N/C nanostructures in an alkaline medium (pH > ~10). Therefore, here the XPS peaks for iron in the WC(30)-FeN_x/C electrocatalysts were deconvoluted into different bands in Fig. 2f corresponding to the peaks at about 710.1 eV and 711.9 eV, which probably reflected the presence of surface Fe^{2+} and Fe^{+3} respectively, [71–74]. As reported by Zhou et al. [75] for a catalyst based on iron oxide, the peaks at 715.3 eV and 718.1 eV corresponded to satellite peaks of Fe^{2+} and Fe^{3+}, respectively. The total amounts of iron was 0.4% in the WC(30)-FeN_x/C(700) catalyst and 0.8% in the WC(30)-FeN_x/C(800) catalyst, indicating that the percentage of Fe^{2+} and Fe^{3+} species are relatively small, but similar in both materials, see Table 1. Even though, the latter electrocatalyst exhibited more surface iron than the former, as well as a smaller amount of nitrogen (2.1%), compared to the material pyrolyzed at 700 °C (2.6%).

3.2. Electrochemical characterization

3.2.1. ORR activities of the tungsten carbides - WC(x)/C

Data in Fig. 3 present the electrochemical responses of the tungsten carbides in a supporting electrolyte of aqueous sulfuric acid saturated with either oxygen or argon. In absence of oxygen (CV) responses (inset in Fig. 3) indicated an absence of redox features of the WC/C nanomaterial in the potential range considered, while addition of O_2 clearly led to the appearance of oxygen reduction currents. The upper limit of the potential scan was limited to 0.8 V in order to minimize the oxidation of WC [52, 53]. The electrocatalytic activities of the WC(x)/C nanomaterials towards the oxygen reduction reaction are illustrated in Fig. 3 through the rotating ring-disk technique at 400 rpm for a 1.0 mg_{cat} cm^{-2}_{disk} (the inset shows the corresponding results for a 0.1 mg_{cat} cm^{-2}_{disk} catalyst layer). The results indicated that WC(30)/C presents higher mass catalytic activities compared to WC(20)/C and to WC(40)/C, as evidenced by the larger currents in the disks containing the same catalyst loading. Fig. 3b shows the effect of the WC(30)/C loading on the release of hydrogen peroxide from the disk electrode. At a low catalyst loading, the percentage of peroxide reaching the ring approached 100% (see also Fig. S5), suggesting that the oxygen reduction reaction on this layer occurred according to a peroxide pathway. Nevertheless, at a high catalyst loading, the percentage of peroxide was drastically reduced, as observed in acidic media for all the tungsten carbides investigated in this work in acid medium. It is interesting to note that a ten times increase in the catalyst loading, from 0.1 mg_{cat} cm^{-2}_{disk} to 1 mg_{cat} cm^{-2}_{disk} (seen inset in Fig. 3a) lead to a ten times increase in current density at about 0.1 V vs RHE, from ~0.15 mA cm^{-2}_{disk} to ~1.5 mA cm^{-2}_{disk}. At a first glance, this proportionality between catalyst loading and current density could have been related to the greater active surface resulting from a higher catalyst loading. However, the results shown in Fig. 3b strongly suggested that the oxygen reduction on the tungsten carbides followed a peroxide pathway, as confirmed by the ring current for the thinner catalyst layer electrode. In the case of a thick electrode (1 mg_{cat} cm^{-2}_{disk}), a significant fraction of the hydrogen peroxide produced could undergo further decomposition, implying that the overall number of electrons involved in the ORR would depended on the thicknesses of the catalyst layer (Fig. 3b) [13]. This observation evidences that not all the catalytic sites in the thick actually electrode are really participated in the electrocatalysis of the ORR.

Data in Fig. 3 and the preceding discussion importantly contribute to the limited understanding of the ORR mechanism on WC, [76] which is suggested here to proceed via a two electrons pathway followed by a decomposition reaction. Furthermore, these results suggest that at potentials of a fuel cell cathode, between about 0.7 V–0.8 vs RHE, oxygen reduction occurring on WC active sites would produce deleterious H_2O_2, e.g. on Pt/WC-C catalysts.

3.2.2. WC(x)-FeN_x/C: impacts of loading and pyrolysis temperature impacts on ORR activity

The data shown in Fig. 4 compare the electrocatalytic activities of the WC(x)-FeN_x/C catalysts towards the oxygen reduction reaction in aqueous sulfuric acid as supporting electrolyte. The catalysts presented various nominal percentages of tungsten carbide (WC(20)/C, WC(30)/C and WC(40)/C) and different pyrolysis temperatures (700 and 800 °C) were employed to incorporate N/C and FeN_x/C active sites [77] in the WC/C structures. The curves in Fig. 4a show the ring-disk currents of the three most active ORR catalysts, prepared at different temperatures of pyrolysis. The hydrogen peroxide oxidation currents on the ring evidence two oxidation peaks, while for the most active catalyst (WC(30)-FeN_x/C(700), the ORR currents in the disk started to approach the limiting current at E < 0.4 V, for the reduction of oxygen to water. The inset in Fig. 4a shows the percentage of hydrogen peroxide produced from the reduction of oxygen on the most active WC-FeN_x/C catalysts. Similar trends can be seen from comparison of these data with

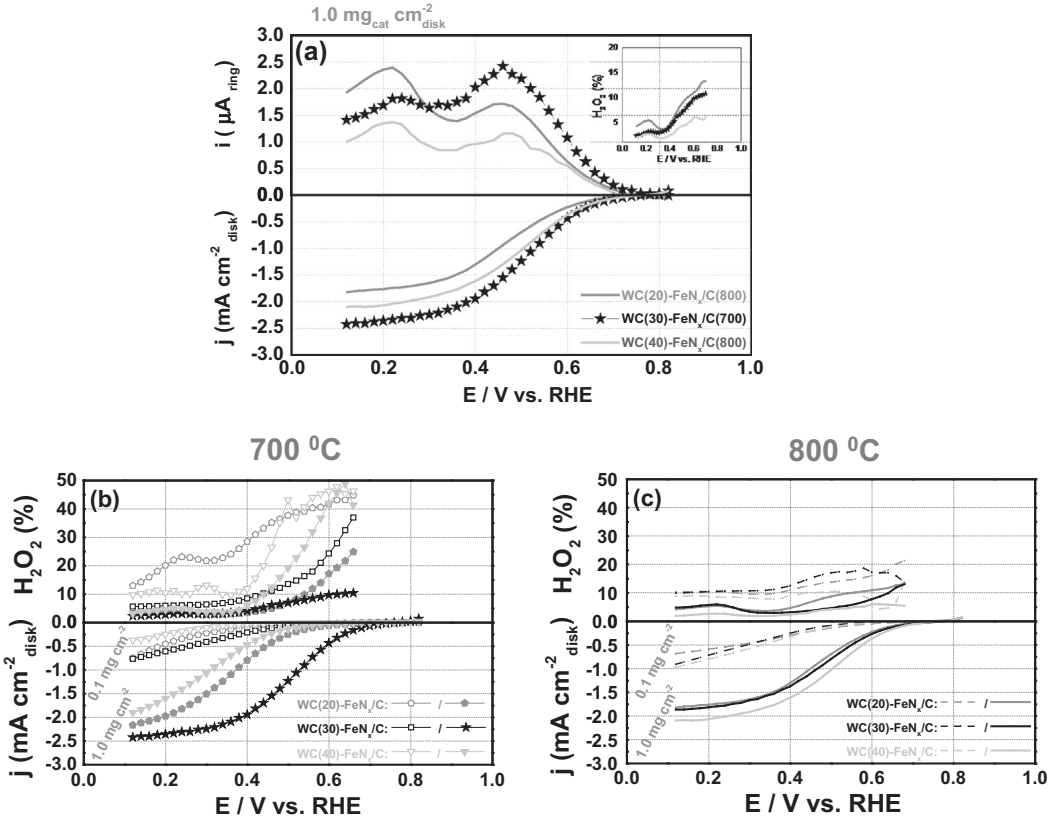

Fig. 4. Electrochemical characterization of the WC(xx)-FeN_x/C(xxx) in 0.5 mol L^{-1} H_2SO_4 with mass loads in the disk of 0.1 mg_{cat} cm^{-2}_{disk} and 1.0 mg_{cat} cm^{-2}_{disk}: (a) ORR polarization responses of the more active electrocatalysts, considering the tungsten carbide contents and pyrolysis temperatures; (b) ORR polarization responses of the WC(xx)-FeN_x/C(700) catalysts; (c) ORR stead state polarization response of the WC(xx)-FeN_x/C(800) catalysts. RRDE experiments performed at a scan rate (v) of 1 mV s^{-1}; w = 400 rpm, T = 25.0 ± 0.1 °C.

those in Fig. 3b for the same catalyst loading (1.0 mg_{cat} cm^{-2}_{disk}). However, in the former case, there was an H_2O_2 oxidation peak at about 0.2 V vs RHE (inset of Fig. 4a), which was not seen for the latter data (Fig. 3b) nor for other Metal-N_x/C catalysts [13, 31, 41–43, 78]. These results suggest the co-existence of different active sites on iron-nitrogen modified tungsten carbide catalysts.

The results for all WC(x)FeN_x/C materials pyrolyzed at 700 and 800 °C are shown in Fig. 4b and c. Similar trends can be seen for all the catalysts, with a greater mass of catalyst on the disk resulting in a smaller amount of hydrogen peroxide detected in the ring, as also observed in Fig. 3b. However, in contrast to the data for the WC/C catalysts (Fig. 3), the results of Fig. 4 indicated that a ten times increase in the mass loading of the FeN_x/C-containing catalysts led to slightly over a two times increases on the ORR limiting current densities measured at ca. 0.1 V vs RHE (Fig. 4b and c, and Fig. S6). This suggested that an additional reduction process contributed to the overall reduction current measured for the thicker electrode layers. This result is in contrast to that on pure WC catalysts (Section 3.2.1), where no further reduction reactions were seen, besides the primarily reduction of oxygen to hydrogen peroxide. This contrast between WC-FeN_x/C and WC/C catalysts suggests that additional active sites are present in the iron-nitrogen modified tungsten carbide nanomaterials, which would reduce hydrogen peroxide to water and would most probably be of the type FeN_x, given that WC were not apparently active for this reaction (Section 3.2.1) and that N/C moieties would be protonated and inactive in acid [43, 79].

In a recent work using high mass transport rates (fuel cell mode) and employing an electrokinetic model, Lopes et al. [13] suggested that the ORR on Metal-N_x/C catalysts might proceed according to a $2e^-$ reduction mechanism producing H_2O_2, at potentials more positive than approximately ~0.750 V vs RHE. The peroxide was subsequently reduced to water at lower potentials. On FeN_x/C active sites, as pointed out by Choi et al. [79] the extent of the second reduction reaction is influenced by the effectiveness of the mass transport of the H_2O_2 away from the electrode, which depends on the thickness of the catalyst layer (as in Fig. 4) and the electrode potential. The results illustrated in Fig. 4b/c indicate that for these hybrid catalysts, oxygen was first reduced to hydrogen peroxide at high potentials on both WC and FeN_x sites. However, the rate of peroxide reduction then increased when the electrode potential approached the standard potential for the reduction of H_2O_2 to water [13, 79], with the percentage of peroxide formed on the thick catalyst layers diminishing to ca. < 10% and being associated with a limiting current for the complete reduction of oxygen to water. Therefore, the present results suggested that the overall oxygen reduction reaction on the WC-FeN_x/C catalysts proceeded according to a $2e^- + 2e^-$ reduction mechanism [13]. This process would first involve the reduction of oxygen to hydrogen peroxide on both ORR active sites, namely WC and FeN_x. However, the second reduction reaction would involve either a further reduction of hydrogen peroxide to water on the FeN_x active site (N/C would be protonated and inactive in acid [43, 79]), or its disproportionation to produce water and oxygen that could again be reduced again to hydrogen peroxide. However, considering the trends in the percentages of hydrogen peroxide as a function of the electrode potential (Figs. 4 and S5) suggested that the chemical disproportionation was less important than the direct reduction of H_2O_2 to water.

Higher ORR catalytic activities were observed for the materials prepared using a higher pyrolysis temperature (Fig. 4b and c), notably for WC(20)-FeN_x/C and WC(40)-FeN_x/C. Consequently, there was a reduction in the amount of hydrogen peroxide detected on the RRDE ring, as clearly observed for the catalyst loading of 0.1 mg_{cat} cm^{2}_{disk}. However, this trend was not followed in the case of the WC(30)-FeN_x/C

catalyst, for which pyrolysis at 700 °C resulted in slightly higher ORR activity, compared to pyrolysis at 800 °C (Fig. 4b and c). Analysis of the elemental compositions of these materials (Table 1 and Table S1) reveled differences in the contents of tungsten, nitrogen and iron contents. The WC(30)-FeN_x/C(800) catalyst contained a smaller content of WC and nitrogen, though a higher concentration of iron in comparison to the WC(30)-FeN_x/C(700) material. A reduction in the WC active site on the surface of the catalyst would lead to a diminished ORR activity, which is also the case for a smaller content of nitrogen required for the formation of FeN_x/C sites that are most active in the ORR in an acidic medium [41]. The results also suggested that the WC(30)-FeN_x/C(700) nanomaterial contained a higher proportion of these active sites [43], hence explaining its higher ORR activity. The fact that FeN_x/C species are also highly active towards the reduction of peroxide to water, [13] could help to explain the smaller percentage of peroxide produced on the WC(30)-N_x/C(700) catalyst, compared to the Fe-free catalyst WC(30)-N_x/C(800), at a catalyst loading of 0.1 $mg_{cat}\,cm_{disk}^{-2}$ (Fig. 4b and c). This result further suggest that FeN_x/C active sites would be the responsible for the reduction of hydrogen peroxide to water on iron-nitrogen modified tungsten carbide nanomaterials, while WC would reduce O_2 to H_2O_2. The pseudo-limiting current density for the ORR on the WC(30)-N_x/C(700) catalyst with a 1.0 mg cat cm_{disk}^{-2} loading was higher than that for the WC(30)-N_x/C(800) electrocatalyst. This was consistent with the higher activity of this material for the reduction of peroxide, as corroborated by its higher pyridinic nitrogen content, which is directly related to FeN_x/C active sites.

Comparison of the ORR activities of the selected catalysts in acidic and alkaline media provided further insights into the oxygen reduction reaction process on the iron-nitrogen modified tungsten carbide nanomaterials. Fig. 5a and b show stead-state polarization curves for the reduction of oxygen on the disk, together with the corresponding currents for the hydrogen peroxide oxidation on the ring, for RRDE experiments conducted in acid (0.5 mol L^{-1} H_2SO_4) and alkaline (0.1 mol L^{-1} NaOH) media on different catalysts, or the WC(30)/C, the WC(30)-FeN_x/C(700), and an Fe-free material, named as WC(30)-N_x/C(700). It can be seen that as the pH increased, there was a clear trend of increasing catalytic activity of the materials, though the limiting current measured is generally similar, denoting a similar reduction mechanism in both pHs. It is also noted a single broad peak corresponding to H_2O_2 formation (insets in Fig. 5a and b), with intensity that depended on the catalyst. The WC(30)-N_x/C(700) catalyst showed the greatest shift in ORR activity with pH. The low activity of this electrocatalyst in an acidic medium can be understood by considering that WC (Fig. 2) and N/C species are not highly active for the ORR at low pHs, [43] and that the ORR active tungsten carbide is largely oxidized to inactive WO_x species following the incorporation of nitrogen by pyrolysis (see the XPS data in Table 1). On the other hand, it has been proposed that N/C active sites are solely for the high ORR activity observed for Metal-N_x/C catalysts at alkaline pHs, [43] which would explain the high activity of the WC(30)-N_x/C(700) electrocatalyst (Fig. 5b). The results shown in Figs. 5 and S7 indicated that the ORR kinetics in acid and alkaline media improved with the incorporation of FeN_x and N/C species in WC/C. The results presented here for WC, WC-N/C and WC-FeN_x/C materials suggest that a significant portion of this improvement could be explained by the presence of the FeN_x moiety in an acidic medium and the N/C moiety at alkaline pH (the high ORR activity in the latter case is further highlighted in Fig. S7). Given the notable activity of the WC(30)-FeN_x/C(700) catalyst (Fig. 5), a comparison with a reference platinum on carbon (Pt/C) catalyst was performed (Fig. 5). This analysis showed that the ORR half-wave potential difference between the hybrid catalyst and Pt/C was ca. 0.060 V in an alkaline medium and of ca. 0.356 V in an acidic medium. These values indicate the promising ORR activity of this class of catalysts and to the high activity of the hybrid material developed here, compared to the few similar materials described in the literature [15–19].

The measured ring currents and hydrogen peroxide percentages

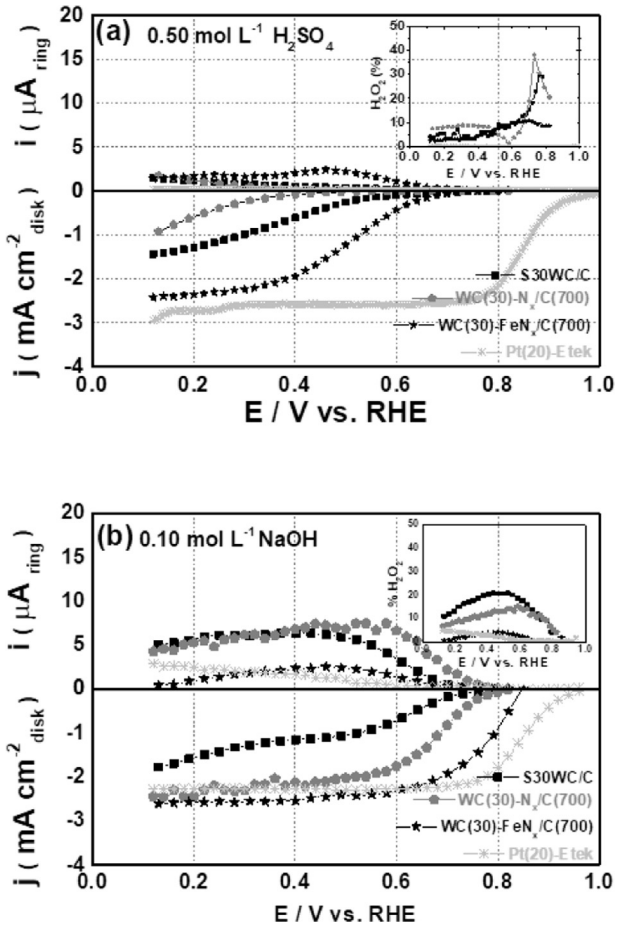

Fig. 5. ORR polarization responses in the disk and corresponding hydrogen peroxide oxidation in the ring for the WC(30)/C, WC(30)-N_x/C(700), WC(30)-FeN_x/C(700) and 20 wt% Pt/C catalysts in (a) 0.5 mol L^{-1} H_2SO_4; (b) 0.1 mol L^{-1} NaOH; (c) percentage of H_2O_2 obtained from the ring currents (see Fig. S6) for WC(30)-FeN_x/C(700) catalyst, in both 0.5 mol L^{-1} H_2SO_4 and 0.1 mol L^{-1} NaOH electrolytes. RRDE experiments performed at a scan rate (v) of 1 mV s^{-1}; w = 400 rpm, T = 25.0 ± 0.1 °C.

(Fig. 5a and b) could be used to gain further insights into the ORR process on these hybrid materials. In an alkaline medium, a three times reduction in the peroxide formation was observed when FeN_x species were introduced into WC(30)-N_x/C(700) to produce the WC(30)-FeN_x/C(700) electrocatalyst (see inset of Fig. 5b), and a similar trend was also observed in an acidic medium (Fig. 5a). These data suggest that in an alkaline medium, the N/C species also efficiently catalyze the reduction of hydrogen peroxide to hydroxide, indicating that the $2e^- + 2e^-$ mechanism is also operates, at least partially, in an alkaline medium. Therefore, the incorporation of FeN_x and N/C moieties on WC/C structures would seem to be a suitable strategy for reducing the release of hydrogen peroxide and producing materials active in the ORR in both acidic and alkaline media.

Fig. 6 shows Tafel curves for the oxygen reduction reaction on the WC(30)/C and WC(30)-FeN_x/C(700) catalysts at two catalyst loadings in acid and alkaline media. These graphs were constructed by correcting the current densities by mass transport processes [33]. Results in Fig. 6a highlights the much smaller ORR activity of the WC(30)/C material, particularly for the electrode with the smaller load. On the other hand, results in Fig. 6b stress the much higher activity of the WC(30)-FeN_x/C(700) catalyst in the alkaline media. In addition, the Tafel values of 160–380 mV dec^{-1} (Fig. 6) were distinct to those observed for platinum catalysts (60–120 mV dec^{-1}) indicating the occurrence of distinct reaction mechanisms and/or differences in terms of number of electrons, reaction order, and/or rate determining steps for the catalysts used in acid or alkaline electrolytes [80, 81].

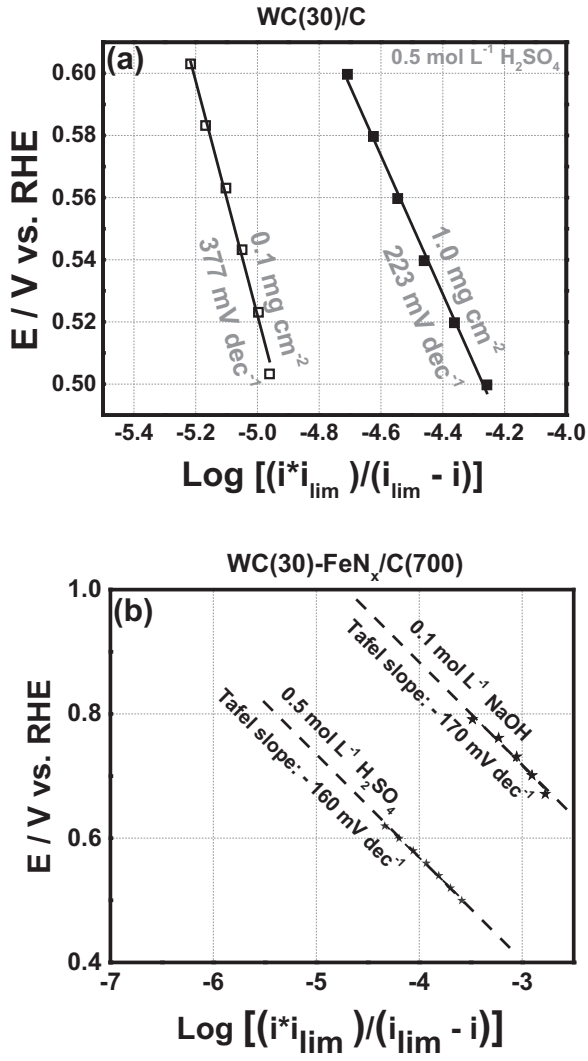

Fig. 6. (a) Mass-transport corrected Tafel plots of the ORR on the WC(30)/C catalyst at low and high catalyst loadings; and (b) corresponding results for the WC(30)-FeN_x/C(700) catalyst, in both acid and alkaline media.

4. Conclusions

Tungsten carbides and transition metal-nitrogen modified tungsten carbide nanomaterials were synthesized and their electrocatalytic activities were evaluated for the oxygen reduction reaction. In-depth analyses using various physical and electrochemical techniques provided insights into the oxygen reduction processes on these materials in both acidic and alkaline media. Suitably ORR active materials were obtained that showed a difference of only about 0.060 V in the ORR half-wave potential in an alkaline medium, compared to a standard platinum catalyst. The results suggested that the oxygen reduction on the tungsten carbides proceeded according to a peroxide pathway and that a significant fraction of the hydrogen peroxide produced might undergo further decomposition along its diffusion through the catalyst layer of WC/C. The data obtained for the hybrid WC-Fe/C catalysts suggested that a significant portion of the ORR improvement observed upon incorporating FeN_x and N/C species on WC/C nanomaterials could have been due to the FeN_x moiety in acidic medium and to the N/C moiety in alkaline pHs, with the reaction mainly following a 2e- + 2e- oxygen reduction mechanism. Each reduction step is suggested to occur on distinct active sites, where in acidic pH, the first process would occur on both WC and FeN_x ORR sites.

Acknowledgements

The authors would like to gratefully thank the Coordenacao de Aperfeicoamento de Pessoal de Nivel Superior (CAPES, process number 1423454) and the Sao Paulo Research Foundation (FAPESP) under process number 2013/16930-7 for financial support. T.L. would also like to thank the Sao Paulo Research Foundation under projects 14/22130-6 and 17/15304-6 for T.L.'s Young Investigator Award and project 2014/09087-4 for assistance during the writing of this manuscript. T.L would also like to acknowledge the support of the RCGI Research Centre for Gas Innovation, sponsored by FAPESP (2014/50279-4) and Shell.

Appendix A. Supplementary data

Supplementary data to this article can be found online at https://doi.org/10.1016/j.jelechem.2018.01.013.

References

[1] S.T. Oyama, P. Clark, X. Wang, T. Shido, Y. Iwasawa, S. Hayashi, J.M. Ramallo-López, F.G. Requejo, Structural characterization of tungsten phosphide (WP) hydrotreating catalysts by X-ray absorption spectroscopy and nuclear magnetic resonance spectroscopy, J. Phys. Chem. B 106 (8) (2002) 1913–1920.
[2] R.B. Levy, M. Boudart, Platinum-like behavior of tungsten carbide in surface catalysis, Science 181 (4099) (1973) 547.
[3] J.G. Chen, Carbide and nitride overlayers on early transition metal surfaces: preparation, characterization, and reactivities, Chem. Rev. 96 (4) (1996) 1477–1498.
[4] L.H. Bennett, J.R. Cuthill, A.J. McAlister, N.E. Erickson, R.E. Watson, Electronic structure and catalytic behavior of tungsten carbide, Science 184 (4136) (1974) 563.
[5] P.N. Ross, P. Stonehart, Surface characterization of catalytically active tungsten carbide (WC), J. Catal. 39 (2) (1975) 298–301.
[6] R.J. Colton, J.-T.J. Huang, J.W. Rabalais, Electronic structure of tungsten carbide and its catalytic behavior, Chem. Phys. Lett. 34 (2) (1975) 337–339.
[7] P.C.K. Vesborg, T.F. Jaramillo, Addressing the terawatt challenge: scalability in the supply of chemical elements for renewable energy, RSC Adv. 2 (21) (2012) 7933–7947.
[8] W. Chu, D. Higgins, Z. Chen, R. Cai, Non-precious Metal Oxides and Metal Carbides for ORR in Alkaline-based Fuel Cells, Non-noble Metal Fuel Cell Catalysts, Wiley-VCH Verlag GmbH & Co, 2014, pp. 357–388 (KGaA).
[9] A. Ishihara, H. Imai, K.-i. Ota, Transition Metal Oxides, Carbides, Nitrides, Oxynitrides, and Carbonitrides for O_2 Reduction Reaction Electrocatalysts for Acid PEM Fuel Cells, Non-noble Metal Fuel Cell Catalysts, Wiley-VCH Verlag GmbH & Co, 2014, pp. 183–204 (KGaA).
[10] F. Jaouen, Heat-Treated Transition Metal-NxCy Electrocatalysts for the O_2 Reduction Reaction in Acid PEM Fuel Cells, Non-noble Metal Fuel Cell Catalysts, Wiley-VCH Verlag GmbH & Co, 2014, pp. 29–118 (KGaA).
[11] D. Singh, J. King, U.S. Ozkan, Modified Carbon Materials for O_2 Reduction Reaction Electrocatalysts in Acid PEM Fuel Cells, Non-noble Metal Fuel Cell Catalysts, Wiley-VCH Verlag GmbH & Co, 2014, pp. 119–156 (KGaA).
[12] D. Banham, S. Ye, Current status and future development of catalyst materials and catalyst layers for proton exchange membrane fuel cells: an industrial perspective, ACS Energy Lett. 2 (3) (2017) 629–638.
[13] T. Lopes, A. Kucernak, D. Malko, E.A. Ticianelli, Mechanistic insights into the oxygen reduction reaction on metal–N–C electrocatalysts under fuel cell conditions, ChemElectroChem 3 (10) (2016) 1580–1590.
[14] M. Shao, Q. Chang, J.-P. Dodelet, R. Chenitz, Recent advances in electrocatalysts for oxygen reduction reaction, Chem. Rev. 116 (6) (2016) 3594–3657.
[15] J.-S. Moon, Y.-W. Lee, S.-B. Han, D.-H. Kwak, K.-H. Lee, A.-R. Park, J.I. Sohn, S.N. Cha, K.-W. Park, Iron-nitrogen-doped mesoporous tungsten carbide nanostructures as oxygen reduction electrocatalysts, Phys. Chem. Chem. Phys. 16 (28) (2014) 14644–14650.
[16] M. Chen, J. Liu, W. Zhou, J. Lin, Z. Shen, Nitrogen-doped Graphene-supported Transition-metals Carbide Electrocatalysts for Oxygen Reduction Reaction, 5 (2015), p. 10389.
[17] S. Bukola, B. Merzougui, A. Akinpelu, M. Zeama, Cobalt and nitrogen co-doped tungsten carbide catalyst for oxygen reduction and hydrogen evolution reactions, Electrochim. Acta 190 (2016) 1113–1123.
[18] H. Zhu, Z. Sun, M. Chen, H. Cao, K. Li, Y. Cai, F. Wang, Highly porous composite based on tungsten carbide and N-doped carbon aerogels for electrocatalyzing oxygen reduction reaction in acidic and alkaline media, Electrochim. Acta 236 (Suppl C) (2017) 154–160.
[19] J. Zhang, J. Chen, Y. Jiang, F. Zhou, G. Wang, R. Wang, Tungsten carbide encapsulated in nitrogen-doped carbon with iron/cobalt carbides electrocatalyst for oxygen reduction reaction, Appl. Surf. Sci. 389 (Suppl C) (2016) 157–164.
[20] J.S. Lee, S.T. Oyama, M. Boudart, Molybdenum carbide catalysts, J. Catal. 106 (1) (1987) 125–133.
[21] P.F. Collins, H. Diehl, G.F. Smith, 2,4,6-tripyridyl-s-triazine as reagent for iron. Determination of iron in limestone, silicates, and refractories, Anal. Chem. 31 (11)

(1959) 1862–1867.
[22] M. Rahsepar, M. Pakshir, P. Nikolaev, Y. Piao, H. Kim, A combined physicochemical and electrocatalytic study of microwave synthesized tungsten mono-carbide nanoparticles on multiwalled carbon nanotubes as a co-catalyst for a proton-exchange membrane fuel cell, Int. J. Hydrog. Energy 39 (28) (2014) 15706–15717.
[23] I.J. Hsu, Y.C. Kimmel, Y. Dai, S. Chen, J.G. Chen, Rotating disk electrode measurements of activity and stability of monolayer Pt on tungsten carbide disks for oxygen reduction reaction, J. Power Sources 199 (2012) 46–52.
[24] T. Dash, B.B. Nayak, Preparation of multi-phase composite of tungsten carbide, tungsten boride and carbon by arc plasma melting: characterization of melt-cast product, Ceram. Int. 42 (1) (2016) 445–459.
[25] E. Cappelli, A. Bellucci, S. Orlando, D.M. Trucchi, A. Mezzi, V. Valentini, PLD deposition of tungsten carbide contact for diamond photodiodes. Influence of process conditions on electronic and chemical aspects, Appl. Surf. Sci. 278 (2013) 111–116.
[26] T. Aoki, T. Matsushita, A. Suzuki, K. Tanabe, M. Okuda, Write-once optical recording using WO_2 films prepared by pulsed laser deposition, Thin Solid Films 509 (1) (2006) 107–112.
[27] W. Yue, S. Wang, Z. Fu, X. Gao, X. Yu, J. Liu, Influence of W content on microstructural, mechanical and tribological properties of sulfurized W-doped diamond-like carbon coatings, Surf. Coat. Technol. 218 (2013) 47–56.
[28] K. Wang, Y. Wang, Y. Tong, Z. Pan, S. Song, A robust versatile hybrid electrocatalyst for the oxygen reduction reaction, ACS Appl. Mater. Interfaces 8 (43) (2016) 29356–29364.
[29] A.P. Grosvenor, B.A. Kobe, M.C. Biesinger, N.S. McIntyre, Investigation of multiplet splitting of Fe 2p XPS spectra and bonding in iron compounds, Surf. Interface Anal. 36 (12) (2004) 1564–1574.
[30] U.A. Paulus, T.J. Schmidt, H.A. Gasteiger, R.J. Behm, Oxygen reduction on a high-surface area Pt/Vulcan carbon catalyst: a thin-film rotating ring-disk electrode study, J. Electroanal. Chem. 495 (2) (2001) 134–145.
[31] T. Lopes, P. Olivi, Non-precious metal oxygen reduction reaction catalysts synthesized via cyanuric chloride and N-ethylamine, Electrocatalysis 5 (4) (2014) 396–401.
[32] F. Dalton, ECS classics: historical origins of the rotating ring-disk electrode, Electrochem. Soc. Interface 25 (3) (2016) 50–59.
[33] M. Lefèvre, J.-P. Dodelet, Fe-based catalysts for the reduction of oxygen in polymer electrolyte membrane fuel cell conditions: determination of the amount of peroxide released during electroreduction and its influence on the stability of the catalysts, Electrochim. Acta 48 (19) (2003) 2749–2760.
[34] K. Jiang, Q. Jia, M. Xu, D. Wu, L. Yang, G. Yang, L. Chen, G. Wang, X. Yang, A novel non-precious metal catalyst synthesized via pyrolysis of polyaniline-coated tungsten carbide particles for oxygen reduction reaction, J. Power Sources 219 (2012) 249–252.
[35] K. Huang, K. Bi, J.C. Xu, C. Liang, S. Lin, W.J. Wang, T.Z. Yang, Y.X. Du, R. Zhang, H.J. Yang, D.Y. Fan, Y.G. Wang, M. Lei, Novel graphite-carbon encased tungsten carbide nanocomposites by solid-state reaction and their ORR electrocatalytic performance in alkaline medium, Electrochim. Acta 174 (2015) 172–177.
[36] T. Ungár, J. Gubicza, G. Ribárik, C. Pantea, T.W. Zerda, Microstructure of carbon blacks determined by X-ray diffraction profile analysis, Carbon 40 (6) (2002) 929–937.
[37] Z.Q. Li, C.J. Lu, Z.P. Xia, Y. Zhou, Z. Luo, X-ray diffraction patterns of graphite and turbostratic carbon, Carbon 45 (8) (2007) 1686–1695.
[38] T. Denaro, V. Baglio, M. Girolamo, V. Antonucci, A.S. Arico', F. Matteucci, R. Ornelas, Investigation of low cost carbonaceous materials for application as counter electrode in dye-sensitized solar cells, J. Appl. Electrochem. 39 (11) (2009) 2173.
[39] Z. Yan, M. Cai, P.K. Shen, Nanosized tungsten carbide synthesized by a novel route at low temperature for high performance electrocatalysis, Sci. Rep. 3 (2013) 1646.
[40] J. Zhang, J. Chen, Y. Jiang, F. Zhou, G. Wang, R. Wang, Tungsten carbide encapsulated in nitrogen-doped carbon with iron/cobalt carbides electrocatalyst for oxygen reduction reaction, Appl. Surf. Sci. 389 (2016) 157–164.
[41] D. Malko, A. Kucernak, T. Lopes, In-situ electrochemical quantification of active sites in Fe-N/C non-precious metal catalysts, Nat. Commun. 7 (2016) 13285.
[42] D. Malko, T. Lopes, E. Symianakis, A.R. Kucernak, The intriguing poison tolerance of non-precious metal oxygen reduction reaction (ORR) catalysts, J. Mater. Chem. A 4 (1) (2016) 142–152.
[43] D. Malko, A. Kucernak, T. Lopes, Performance of Fe–N/C oxygen reduction electrocatalysts toward NO2–, NO, and NH_2OH electroreduction: from fundamental insights into the active center to a new method for environmental nitrite destruction, J. Am. Chem. Soc. 138 (49) (2016) 16056–16068.
[44] H. Shen, E. Gracia-Espino, J. Ma, H. Tang, X. Mamat, T. Wagberg, G. Hu, S. Guo, Atomically FeN_2 moieties dispersed on mesoporous carbon: a new atomic catalyst for efficient oxygen reduction catalysis, Nano Energy (2017), http://dx.doi.org/10.1016/j.nanoen.2017.03.027.
[45] J.H. Kim, Y.J. Sa, H.Y. Jeong, S.H. Joo, Roles of Fe-Nx and Fe-Fe3C@C species in Fe-N/C electrocatalysts for oxygen reduction reaction, ACS Appl. Mater. Interfaces 9 (11) (2017) 9567–9575.
[46] M. Wang, T. Qian, J. Zhou, C. Yan, An efficient bifunctional electrocatalyst for a zinc-air battery derived from Fe/N/C and bimetallic metal-organic framework composites, ACS Appl. Mater. Interfaces 9 (6) (2017) 5213–5221.
[47] M.A.P. Almeida, L.S. Cavalcante, C. Morilla-Santos, C.J. Dalmaschio, S. Rajagopal, M.S. Li, E. Longo, Effect of partial preferential orientation and distortions in octahedral clusters on the photoluminescence properties of $FeWO_4$ nanocrystals, CrystEngComm 14 (21) (2012) 7127–7132.
[48] A. Lavacchi, H. Miller, F. Vizza, Carbon-based Nanomaterials, Nanotechnology in Electrocatalysis for Energy, Springer New York, New York, NY, 2013, pp. 115–144.
[49] L. Rapoport, N. Parkansky, I. Lapsker, A. Rayhel, B. Alterkop, R.L. Boxman, S. Goldsmith, L. Burstain, Effect of transverse current injection on the tribological properties of WC cemented carbide, Wear 249 (1–2) (2001) 1–5.
[50] L. Jiang, H. Fu, L. Wang, G. Mu, B. Jiang, W. Zhou, R. Wang, Tungsten carbide/porous carbon composite as superior support for platinum catalyst toward methanol electro-oxidation, Mater. Res. Bull. 49 (2014) 480–486.
[51] Y. Liu, W.E. Mustain, Evaluation of tungsten carbide as the electrocatalyst support for platinum hydrogen evolution/oxidation catalysts, Int. J. Hydrog. Energy 37 (11) (2012) 8929–8938.
[52] M.C. Weidman, D.V. Esposito, I.J. Hsu, J.G. Chen, Electrochemical stability of tungsten and tungsten monocarbide (WC) over wide pH and potential ranges, J. Electrochem. Soc. 157 (12) (2010) F179–F188.
[53] M.C. Weidman, D.V. Esposito, Y.-C. Hsu, J.G. Chen, Comparison of electrochemical stability of transition metal carbides (WC, W2C, Mo2C) over a wide pH range, J. Power Sources 202 (2012) 11–17.
[54] P.J. Kulesza, B. Grzybowska, M.A. Malik, M.T. Galkowski, Tungsten oxides as active supports for highly dispersed platinum microcenters: electrocatalytic reactivity toward reduction of hydrogen peroxide and oxygen, J. Electrochem. Soc. 144 (6) (1997) 1911–1917.
[55] C.A. Ma, Y. Jin, M. Shi, Y. Chu, Y. Xu, W. Jia, Q. Yuan, J. Chen, D. Chen, S. Chen, Study of nano-WO3 modified carbon nanotubes supported Pt electrocatalyst for oxygen reduction reaction, J. Electrochem. Soc. 161 (3) (2014) F246–F251.
[56] T. Tuvić, I. Pašti, S. Mentus, Tungsten electrochemistry in alkaline solutions—anodic dissolution and oxygen reduction reaction, Russ. J. Phys. Chem. A 85 (13) (2011) 2399–2405.
[57] J.L. Bott-Neto, W. Beck, L.C. Varanda, E.A. Ticianelli, Electrocatalytic activity of platinum nanoparticles supported on different phases of tungsten carbides for the oxygen reduction reaction, Int. J. Hydrog. Energy 42 (32) (2017) 20677–20688.
[58] X. Zhou, Y. Qiu, J. Yu, J. Yin, S. Gao, Tungsten carbide nanofibers prepared by electrospinning with high electrocatalytic activity for oxygen reduction, Int. J. Hydrog. Energy 36 (13) (2011) 7398–7404.
[59] A.R. Ko, Y.-W. Lee, J.-S. Moon, S.-B. Han, G. Cao, K.-W. Park, Ordered mesoporous tungsten carbide nanoplates as non-Pt catalysts for oxygen reduction reaction, Appl. Catal. A Gen. 477 (Suppl C) (2014) 102–108.
[60] K. Huang, K. Bi, J.C. Xu, C. Liang, S. Lin, W.J. Wang, T.Z. Yang, Y.X. Du, R. Zhang, H.J. Yang, D.Y. Fan, Y.G. Wang, M. Lei, Novel graphite-carbon encased tungsten carbide nanocomposites by solid-state reaction and their ORR electrocatalytic performance in alkaline medium, Electrochim. Acta 174 (Suppl C) (2015) 172–177.
[61] W. Ding, Z. Wei, S. Chen, X. Qi, T. Yang, J. Hu, D. Wang, L.-J. Wan, S.F. Alvi, L. Li, Space-confinement-induced synthesis of pyridinic- and pyrrolic-nitrogen-doped graphene for the catalysis of oxygen reduction, Angew. Chem. Int. Ed. 52 (45) (2013) 11755–11759.
[62] J.R. Pels, F. Kapteijn, J.A. Moulijn, Q. Zhu, K.M. Thomas, Evolution of nitrogen functionalities in carbonaceous materials during pyrolysis, Carbon 33 (11) (1995) 1641–1653.
[63] I. Kusunoki, M. Sakai, Y. Igari, S. Ishidzuka, T. Takami, T. Takaoka, M. Nishitani-Gamo, T. Ando, XPS study of nitridation of diamond and graphite with a nitrogen ion beam, Surf. Sci. 492 (3) (2001) 315–328.
[64] E. Raymundo-Piñero, D. Cazorla-Amorós, A. Linares-Solano, J. Find, U. Wild, R. Schlögl, Structural characterization of N-containing activated carbon fibers prepared from a low softening point petroleum pitch and a melamine resin, Carbon 40 (4) (2002) 597–608.
[65] S. Maldonado, S. Morin, K.J. Stevenson, Structure, composition, and chemical reactivity of carbon nanotubes by selective nitrogen doping, Carbon 44 (8) (2006) 1429–1437.
[66] D. Guo, R. Shibuya, C. Akiba, S. Saji, T. Kondo, J. Nakamura, Active sites of nitrogen-doped carbon materials for oxygen reduction reaction clarified using model catalysts, Science 351 (6271) (2016) 361.
[67] J. Liu, P. Song, W. Xu, Structure-activity relationship of doped-nitrogen (N)-based metal-free active sites on carbon for oxygen reduction reaction, Carbon 115 (2017) 763–772.
[68] J. Liu, P. Song, M. Ruan, W. Xu, Catalytic properties of graphitic and pyridinic nitrogen doped on carbon black for oxygen reduction reaction, Chin. J. Catal. 37 (7) (2016) 1119–1126.
[69] U.I. Kramm, I. Herrmann-Geppert, J. Behrends, K. Lips, S. Fiechter, P. Bogdanoff, On an easy way to prepare metal-nitrogen doped carbon with exclusive presence of MeN4-type sites active for the ORR, J. Am. Chem. Soc. 138 (2) (2016) 635–640.
[70] A. Zitolo, V. Goellner, V. Armel, M.-T. Sougrati, T. Mineva, L. Stievano, E. Fonda, F. Jaouen, Identification of catalytic sites for oxygen reduction in iron- and nitrogen-doped graphene materials, Nat. Mater. 14 (9) (2015) 937–942.
[71] T. Mathew, N.R. Shiju, V.V. Bokade, B.S. Rao, C.S. Gopinath, Selective catalytic synthesis of 2-ethyl phenol over Cu1-xCox Fe_2O_4-kinetics, catalysis and XPS aspects, Catal. Lett. 94 (3) (2004) 223–236.
[72] T. Mathew, S. Shylesh, B.M. Devassy, M. Vijayaraj, C.V.V. Satyanarayana, B.S. Rao, C.S. Gopinath, Selective production of orthoalkyl phenols on Cu0.5Co0.5Fe_2O_4: a study of catalysis and characterization, Appl. Catal. A Gen. 273 (1–2) (2004) 35–45.
[73] M. Vijayaraj, C.S. Gopinath, On the “active spacer and stabilizer” role of Zn in Cu1-xZnxFe2O4 in the selective mono-N-methylation of aniline: XPS and catalysis study, J. Catal. 241 (1) (2006) 83–95.
[74] T. Yamashita, P. Hayes, Analysis of XPS spectra of Fe2+ and Fe3+ ions in oxide materials, Appl. Surf. Sci. 254 (8) (2008) 2441–2449.
[75] C. Zhou, L. Sun, A. Zhang, X. Wu, C. Ma, S. Su, S. Hu, J. Xiang, Fe_3-xCuxO_4 as highly active heterogeneous Fenton-like catalysts toward elemental mercury removal, Chemosphere 125 (2015) 16–24.
[76] C. Song, J. Zhang, Electrocatalytic oxygen reduction reaction, in: J. Zhang (Ed.), PEM Fuel Cell Electrocatalysts and Catalyst Layers: Fundamentals and Applications, Springer London, London, 2008, pp. 89–134.

[77] K. Strickland, E. Miner, Q. Jia, U. Tylus, N. Ramaswamy, W. Liang, M.-T. Sougrati, F. Jaouen, S. Mukerjee, Highly Active Oxygen Reduction Non-platinum Group Metal Electrocatalyst Without Direct Metal–Nitrogen Coordination, vol. 6, (2015), p. 7343.
[78] A.R.J. Kucernak, T. Lopes, D. Malko, WO2015049318 A1 Oxygen Reduction Catalysts, (2015).
[79] C.H. Choi, W.S. Choi, O. Kasian, A.K. Mechler, M.T. Sougrati, S. Brüller, K. Strickland, Q. Jia, S. Mukerjee, K.J.J. Mayrhofer, F. Jaouen, Unraveling the nature of sites active toward hydrogen peroxide reduction in Fe-N-C catalysts, Angew. Chem. Int. Ed. (2017), http://dx.doi.org/10.1002/anie.201704356.
[80] G. Inzelt, Kinetics of electrochemical reactions, in: F. Scholz, A.M. Bond, R.G. Compton, D.A. Fiedler, G. Inzelt, H. Kahlert, Š. Komorsky-Lovrić, H. Lohse, M. Lovrić, F. Marken, A. Neudeck, U. Retter, F. Scholz, Z. Stojek (Eds.), Electroanalytical Methods: Guide to Experiments and Applications, Springer Berlin Heidelberg, Berlin, Heidelberg, 2010, pp. 33–53.
[81] A. Bard, L. Faulkner, Kinetics of Electrode Reactions in Electrochemical Methods: Fundamentals and Applications, John Wiley & Sons, Inc, 2001, pp. 87–136.